Microtubule polarity is instructive for many aspects of neuronal polarity

Pankajam Thyagarajan[1], **Chengye Feng**[1,2], **David Lee**[1,3], **Matthew Shorey**[1], **Melissa M. Rolls**[1]

[1]Biochemistry and Molecular Biology and the Huck Institutes of the Life Sciences, The Pennsylvania State University, University Park, PA 16802

[2]Current address: Yale University School of Medicine ++

[3]Current address: University of North Carolina ++

Abstract

Many neurons in bilaterian animals are polarized with functionally distinct axons and dendrites. Microtubule polarity, microtubule stability, and the axon initial segment (AIS) have all been shown to influence polarized transport in neurons. Each of these cytoskeletal cues could act independently to control axon and dendrite identity, or there could be a hierarchy in which one acts upstream of the others. Here we test the hypothesis that microtubule polarity acts as a master regulator of neuronal polarity by using a Drosophila genetic background in which some dendrites have normal minus-end-out microtubule polarity and others have the axonal plus-end-out polarity. In these mosaic dendrite arbors, we found that ribosomes, which are more abundant in dendrites than axons, are reduced from plus-end-out dendrites, while an axonal cargo was increased. In addition, we determined that microtubule stability was different in plus-end-out and minus-end-out dendrites, with plus-end-out ones having more stable microtubules like axons. Similarly, we found that ectopic diffusion barriers, like those at the AIS, formed at the base of dendrites with plus-end-out regions. Thus, changes in microtubule polarity were sufficient to rearrange other cytoskeletal features associated with neuronal polarization. However, overall neuron shape was maintained with only subtle changes in branching in mosaic arbors. We conclude that microtubule polarity can act upstream of many aspects of intracellular neuronal polarization, but shape is relatively resilient to changes in microtubule polarity in vivo.
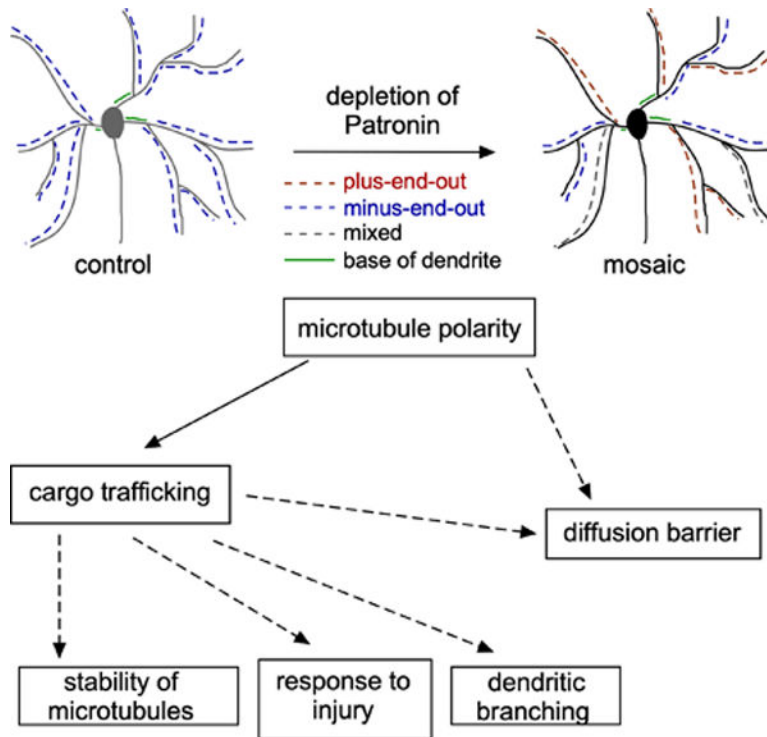
Graphical Abstract

Introduction

A hallmark feature of most neurons in animals with centralized nervous systems is the ability to make two types of neurites: axons and dendrites (Craig and Banker, 1994; Rolls and Jegla, 2015). This polarization enables efficient, directional information flow, with dendrites receiving and integrating signals and axons sending them. This functional specialization requires different sets of proteins and organelles to be present in the two compartments, for example dendrites need receptors and axons need synaptic vesicles. Most new proteins are synthesized in the cell body, so this means that directed transport from a single point of origin is important for efficiently populating axons and dendrites with correct contents. In addition to differences closely linked to directional signaling, axons and dendrites are often distinguished in less intuitive ways. For example, dendrites tend to branch closer to the cell body and to taper as they branch, while axons often branch only near their target maintain similar caliber throughout (Craig and Banker, 1994). Dendrites tend to have more synthetic capability than axons, with pockets of ribosomes and Golgi outposts that are rare or absent in axons (Bartlett and Banker, 1984; Craig and Banker, 1994; Horton et al., 2005). Axons and dendrites can also contain different sets of cytoskeletal proteins, with a classic example being concentration of microtubule-binding proteins MAP2 in dendrites and tau in axons (Craig and Banker, 1994). Axonal microtubules are also more stable than dendritic ones (Kollins et al., 2009; Rolls et al., 2020). How is this complex set of

features that distinguish axons and dendrites orchestrated? One possibility is that there is a hierarchical regulatory system with a single master regulator. Alternatively, several different mechanisms may operate in parallel to confer specific features to axons and dendrites.

One candidate for a master regulator of axon and dendrite identity is microtubule polarity. Axonal microtubules have their more dynamic plus ends growing away from the cell body (Baas and Lin, 2011; Rolls and Jegla, 2015; van Beuningen and Hoogenraad, 2016). In contrast, dendrites typically contain a significant proportion of microtubules with minus ends distal to the cell body (minus-end-out). In mammalian neurons, dendrite polarity is mixed (Baas et al., 1988; Stepanova et al., 2003; Tas et al., 2017; Yau et al., 2016), while dendrites in C. elegans and Drosophila can be populated almost completely by minus-end-out microtubules (Goodwin et al., 2012; Harterink et al., 2018; Rolls et al., 2007; Stone et al., 2008; Yan et al., 2013). This difference in microtubule polarity could be used to steer specific components into axons and dendrites and direct differentiation of the two compartments. Indeed, there is substantial evidence supporting a role for minus-end-out microtubules in establishing dendrite identity. Knockdown of kinesin-6 results in loss of minus-end-out microtubules in cultured mammalian neurons. Early knockdown blocks dendrite formation (Lin et al., 2012; Sharp et al., 1997), and knockdown after dendrite formation causes loss of dendritic morphology, MAP2 and ribosomes (Yu et al., 2000). Similar observations have been made in C. elegans where reduction of kinesin-1 causes normally minus-end-out dendrites to take on plus-end-out axonal polarity (Yan et al., 2013) and results in loss of dendritic markers and entry of axonal ones into the affected neurite (Yan et al., 2013). Thus, evidence from mammalian neurons in culture and C. elegans neurons in vivo suggests that, at minimum, microtubule polarity is an important determinant of delivery of dendrite-specific cargoes. However, whether it is a master regulator of polarity is less clear.

Microtubule stability distinguishes axons and dendrites in mammalian and Drosophila neurons, with axonal microtubules being more stable than dendritic ones (Baas et al., 2016; Baas et al., 1991; Rolls et al., 2020). In cultured neurons, stabilizing microtubules during neurite outgrowth results in formation of multiple axons (Witte et al., 2008) suggesting that stability can act upstream of microtubule polarity. Differences in stability, or more specifically post-translational modifications associated with more stable microtubules, can also direct cargo carried by some kinesins to axons (Hammond et al., 2010). Therefore, microtubule stability is an alternate candidate for a master regulator of neuronal polarity, instructing microtubule polarity as well as helping deliver cargoes to the correct compartment.

Another candidate for an independent regulator of polarized transport and neurite identity is the axon initial segment. In addition to concentrating channels for action potential initiation, the axon initial segment (AIS) serves as a physical barrier that separates the axonal and dendritic plasma membranes to maintain distinct surface composition (Winckler et al., 1999). In mammals, giant isoforms of ankyrin G orchestrate formation and function of the AIS (Rasband, 2010) and loss of ankyrin G allows dendritic components, including dendritic spines, to leak into axons (Hedstrom et al., 2008). Although best established as a barrier for the plasma membrane, the AIS may also restrict entry of cytoplasmic material into the

axon (Song et al., 2009). While this structure was proposed to be vertebrate-specific because ankyrin G could not be identified in invertebrates based on sequence (Jenkins et al., 2015), it is now known that giant ankyrins also organize a plasma membrane diffusion barrier at the base of Drosophila axons suggesting that the AIS is a general feature of bilaterian neurons (Jegla et al., 2016a). While it is unlikely that the AIS acts upstream of microtubule polarity as it forms after differences in polarity are established in axons and dendrites (Jegla et al., 2016a; Nakada et al., 2003), it may act in parallel to microtubules to distinguish axons and dendrites.

To probe the relationship between microtubule polarity, stability, and the axonal diffusion barrier in the context of neuronal polarity, we used a Drosophila genetic background that disrupts minus-end-out polarity of dendrites. Patronin is the Drosophila CAMSAP protein, and binds minus ends of microtubules (Goodwin and Vale, 2010). In neurons, it is required for sustained growth of minus ends (Feng et al., 2019). During dendrite development, minus ends grow into dendrites from the cell body, and this contributes to establishment of minus-end-out polarity (Feng et al., 2019). When Patronin is reduced ddaC neurons, which have large dendrite arbors that sense noxious touch in the skin (Grueber et al., 2002; Hwang et al., 2007), some regions of the arbor establish normal minus-end-out polarity, while other branches take on the axonal plus-end-out polarity (Feng et al., 2019). We first characterize these mosaic neurons in more detail, and then assay localization of axonal and dendritic cargoes in plus-end-out and minus-end-out regions of the same arbor. Finally, we show that microtubule stability and establishment of AIS-like diffusion barriers are controlled by microtubule polarity. In contrast to intracellular features, dendrite shape was largely unaffected by microtubule polarity changes. We conclude that microtubule polarity acts upstream of a cytoskeletal hierarchy that establishes intracellular organization of axons and dendrites.

Results

Reduction of Patronin generates mosaic dendrite arbors with plus-end-out and minus-end-out regions emerging from minus-end-out bases.

Drosophila dendritic arborization neurons are sensory neurons with branched dendrites that receive mechanosensory information in the skin and send it via axons to the central nervous system (Grueber et al., 2002). Although their dendrites are not postsynaptic, they have classic dendritic features including Golgi outposts (Ye et al., 2007), ribosomes (Hill et al., 2012) and minus-end-out microtubules (Rolls et al., 2007; Stone et al., 2008). Class IV dendritic arborization neurons, including the ddaC cell, have the largest arbors (Grueber et al., 2002) and in larvae allow the animal to sense parasitic wasps and initiate an escape response (Hwang et al., 2007). Like other Drosophila neurons, ddaC dendrites contain predominantly minus-end-out microtubules (Ori-McKenney et al., 2012; Rolls et al., 2007; Stone et al., 2008). When extended growth of microtubule minus ends is reduced in ddaC cells by Patronin RNAi, only about half of the major dendrite branches have normal minus-end-out microtubule polarity, with the other half split between mixed microtubule polarity and plus-end-out polarity (Feng et al., 2019; Wang et al., 2019). Axons in these neurons do not exhibit polarity changes (Feng et al., 2019). Patronin is the sole

Drosophila representative of the Patronin/CAMSAP family of proteins. These proteins specifically recognize uncapped microtubule minus ends and track and/or stabilize them (Goodwin and Vale, 2010; Hendershott and Vale, 2014; Jiang et al., 2014). In Drosophila neurons, Patronin-facilitated minus end growth helps populate dendrites with minus-end-out microtubules (Feng et al., 2019).

To determine whether Patronin RNAi might be useful for assaying the role of microtubule polarity on axon-dendrite differentiation, we characterized microtubule organization in more detail in knockdown ddaC neurons. Microtubule polarity was visualized with EB1-GFP, which binds growing microtubule ends. The direction of plus end growth can be used to map polarity of the microtubule array (Stepanova et al., 2003). In major branches of control ddaC neurons, over 90% of microtubules are minus-end-out (Feng et al., 2019; Ori-McKenney et al., 2012) (Figure 1B and 1C). We expressed a hairpin RNAi targeting Patronin using two different Gal4 drivers specific to Class IV neurons, 477 and ppk; in our experience ppk drives higher expression than 477. Three different RNAi lines were previously shown to have a similar phenotype (Feng et al., 2019). In this study we used one of these three that is a short hairpin so does not require added dicer2 to give neuronal knockdown; this reduced the number of transgenes needed for experiments.

As previously described (Feng et al., 2019), knockdown of Patronin yielded dendrite arbors with regionally different microtubule polarity (Figure 1 and Video 1). At the global level, some dendrite branches had minus-end-out polarity (>90% minus-end-out), some were mixed, and some had plus-end-out polarity (>90% plus-end-out) (Figure 1C). At the level of individual neurons, most cells contained all three types of branches (Figure 1H). Plus-end-out branches were more common when knockdown was driven with ppk (Figure 1H), consistent with this driving stronger expression than 477. One interesting observation was that the region of the dendrite between the cell body and first branchpoint, the base, was almost always minus-end-out (Figure 1D). Plus-end-out and minus-end-out regions of dendrites did not exhibit grossly different major branching patterns (Figure 1A and 1E). We could therefore compare structurally similar dendritic regions with similar extracellular context, but different microtubule polarity, to try to isolate the effect of microtubule organization on other aspects of dendrite identity. We term these dendrites mosaic, as a single arbor is made up of distinct regions (Figure 1G).

To facilitate use of mosaic dendrite arbors, we generated a Drosophila line that contained the ppk-Gal4 driver, UAS-EB1-TagRFP-T and the short hairpin UAS-Patronin-RNAi. EB1-TagRFP-T allows us to determine the polarity of each region of the dendrite arbor. We could cross flies from this line to those from lines with GFP transgenes to analyze a variety of features associated with axon and dendrite identity.

Microtubule polarity predicts polarized cargo distribution.

Based on experiments in mammalian and worm neurons, we anticipated that cargo delivery would be sensitive to changes in microtubule polarity. We therefore began by assaying axon and dendrite-specific cargo localization in mosaic dendrite arbors. We used ANF-GFP, a marker for neuropeptide-containing dense core vesicles (Wong et al., 2012), that is largely excluded from dendrites of dendritic arborization neurons (Hill et al., 2012) as an axonal

marker. In control ddaC neurons, ANF-GFP was abundant in the cell body, and could be seen along the axon (Figure 2A). While some puncta entered the base of the dendrite, very few were visible beyond the first branch point. To analyze its distribution in mosaic dendrite arbors, it was crossed to the ppk-Gal4, UAS-EB1-TagRFP-T, UAS-Patronin RNAi line. In mosaic neurons, ANF-GFP was present in the axon as in control cells, but puncta also accumulated in distal regions of a subset of dendrites (Figure 2C). Microtubule polarity of dendrite branches was determined from movies of EB1 (Figure 2D), and then compared to the pattern of ANF-GFP. Both mixed and plus-end-out dendrites contained ANF-GFP, while minus-end-out ones rarely did (Figure 2B and 2C). This suggests that the presence of a population of plus-end-out microtubules allows an axonal cargo to accumulate in dendrites, even when the plus-end-out region occurs beyond a minus-end-out one (Figure 2E).

Based on the accumulation of axonal cargoes in any neurite with plus-end-out microtubules, we hypothesized that a dendritic cargo would localize to minus-end-out and mixed polarity dendrites, but not plus-end-out ones. To test this hypothesis, we monitored ribosome localization. Ribosomal protein L10 tagged with YFP (YFP-L10) localizes to the cell body and dendrite branch points in dendritic arborization neurons (Hill et al., 2012). In control ddaC neurons, accumulation of YFP-L10 was seen at most dendrite branch points (Figure 3A). In mosaic arbors, we used EB1-TagRFP-T to identify regions with different polarity, and quantitated YFP-L10 fluorescence intensity at branch points. While we could still detect some L10 at branch points of plus-end-out dendrites, the intensity was lower than in minus-end-out branch points (Figure 3). Surprisingly, dendrite branches with mixed polarity had similar low levels of YFP-L10 at branch points as plus-end-out branches (Figure 3D). We conclude that microtubule polarity can instruct accumulation of axon and dendrite cargoes, but mixed polarity can be interpreted in different ways depending on the cargo.

Microtubule orientation acts upstream of microtubule stability

Having confirmed that microtubule polarity can direct accumulation of axon and dendrite-specific contents, we wished to determine whether it might control other aspects of cytoskeletal polarity that differentiate axons and dendrites. We began by examining microtubule stability. In ddaC neurons, dendritic microtubules turnover more quickly than axonal ones in a photoconversion assay (Rolls et al., 2020). ddaC dendrites also have more growing plus ends per unit length than axons (Hertzler et al., 2020), consistent with the interpretation that dendritic microtubules are shorter, and thus less stable, than axonal ones. We confirmed that control ddaC neurons have fewer EB1-GFP comets per length in axons than dendrites (Figure 4A and B).

To test whether microtubule orientation acts upstream of stability, we assayed comet number in mosaic dendrite arbors. Minus-end-out branches had very similar numbers of microtubule plus ends per length to control dendrites, while plus-end-out regions were comparable to axons (Figure 4A and 4B). One caveat to this type of analysis is that the number of plus ends per unit length only accurately reflects microtubule length if the same amount of polymerized tubulin is present in the regions for comparison; ie axons could contain fewer growing plus ends per unit length if they had fewer microtubules in any cross section than dendrites. To make sure that this was not the explanation for the difference in plus

end numbers between plus-end-out and minus-end-out regions of mosaic arbors, we paired analysis of comet numbers with a measure of total amount of microtubules. We used tdEOS-tagged α-Tubulin as a measure of microtubule polymer in a region (Figure 4C). To make sure that tdEOS-α-Tubulin is a reasonable measure of microtubule mass in dendrites, we compared its distribution at dendrite branch points to that of a soluble fluorescent protein (Figure 4E). The soluble fluorescent protein, iBlueberry (Yu et al., 2016) filled the volume of the branch, while tdEOS-α-Tubulin was almost exclusively seen at the edges of the branch where microtubule bundles run. Thus, the tdEOS-α-Tubulin signal is primarily derived from microtubule polymer rather than free tubulin. To normalize comet number to tubulin polymer, we expressed tdEOS-α-Tubulin and EB1-TagRFP-T together in ddaC neurons. We took movies in which we could simultaneously measure the intensity of tdEOS-α-Tubulin and comet number and direction (Figure 4D). When amount of tagged tubulin was taken into account, fewer EB1 comets per unit length were present in plus-end-out regions of the arbor compared to minus-end-out ones (Figure 4F). Thus, the difference in comet number in plus-end-out and minus-end-out regions (Figure 4G) is likely because microtubules in plus-end-out branches are longer and more stable than in minus-end-out regions. These results are consistent with microtubule polarity directing microtubule stability in neurons.

Injury-induced dynamics depends on microtubule polarity.

The difference in comet number in plus and minus-end-out dendrite branches suggested that many aspects of microtubule behavior might be influenced by polarity. If axons and dendrites are severed from the cell body, the cut off region can no longer function and is actively disassembled. An early step in injury-induced dendrite degeneration is microtubule severing by the AAA-ATPase fidgetin (Tao et al., 2016). In neurons expressing EB1-GFP, this results in an increase in comet number in the cut off dendrite during the first hour after severing (Tao et al., 2016). To make sure that this increase in microtubule dynamics in severed regions was specific to dendrites, we examined plus end number in dendrites and axons before and after severing (Figure 5A and 5C). In severed dendrites, comet density often increased one hour after injury (Figure 5B). In contrast, comet density in severed axons always decreased (Figure 5D). To compare outcomes, we categorized the response of individual neurites into two bins: 1- comet number increased, or 2- comet number did not increase. Using a Fisher's exact test the response to injury was significantly different in axons and dendrites (p<0.05). Next, we compared microtubule dynamics in severed neurites of mosaic arbors (Figure 5E). The pattern of response in minus-end-out neurites was very similar to that in control dendrites, with a subset increasing comet number (Figure 5F). In contrast, the plus-end-out neurites never showed an increase in the number of EB1-GFP comets (Figure 5F) similar to axons. We performed a similar analysis to that in control neurons by binning outcomes into two categories and compared responses with a Fisher's exact test. As with the axon vs. dendrite comparison above, the outcome was different between plus-end-out and minus-end-out dendrite branches (p<0.05). Thus, the dynamics of microtubules in severed pieces of dendrites depends on polarity within that branch.

Ectopic diffusion barriers form in mosaic dendrite arbors.

So far, we have shown that plus-end-out regions of mosaic dendrite arbors accumulate axonal cargoes and have microtubule stability before and after injury similar to that of axons. We wanted to determine whether another distinguishing feature of the axon, the diffusion barrier at the AIS, might also respond to microtubule polarity. In Drosophila dendritic arborization neurons, a diffusion barrier forms at the base of the axon, immediately adjacent to the cell body and, as in mammalian neurons, this depends on giant ankyrin isoforms (Jegla et al., 2016a). We first tested whether reduction of Patronin affected the axonal diffusion barrier. As in our previous study (Jegla et al., 2016a), we used a general plasma membrane marker, mCD8-GFP, to monitor fluorescence recovery after photobleaching (FRAP). Very little recovery was observed in proximal axons in control or Patronin RNAi neurons (Figure 6) indicating that a normal diffusion barrier is established in neurons with mosaic arbors. This contrasts with rapid recovery in a similar region at the base of dendrites in control neurons (Figure 6 and (Jegla et al., 2016a)).

As the axonal diffusion barrier is positioned at the beginning of plus-end-out axons, we hypothesized that if a diffusion barrier forms in plus-end-out regions of mosaic arbors, then it would be positioned at the base of the plus-end-out branch. We used EB1-TagRFP-T movies to identify plus-end-out branches in mosaic dendrite arbors and bleached mCD8-GFP at the base of the branch. As the region of the dendrite emerging from the cell body was almost always minus-end-out (Figure 1D), this meant bleaching just beyond the first branch point (Figure 6A, second row). Fluorescence recovered very quickly into the region indicating that no diffusion barrier forms where plus-end-out polarity initiates (Figure 6, second row). Because the axonal diffusion barrier forms at the exit from the cell body, we also performed bleaching in mosaic dendrites in an analogous position. Surprisingly, mCD8-GFP diffusion was extremely limited in this proximal position, and was indistinguishable from that in the axon (Figure 6). Thus plus-end-out polarity in distal regions of the dendrite arbor directs establishment of a diffusion barrier in the initial region of the dendrite, even though this segment has minus-end-out polarity.

Plus-end-out neurites in mosaic arbors have reduced branching.

Plus-end-out polarity seems sufficient to direct axonal cargoes to dendrites, cause microtubules to take on axonal stability, and can establish extra diffusion barriers. However, plus-end-out regions of dendrite arbors still innervate the body wall in a pattern very similar to their minus-end-out neighboring branches (Figure 7A) despite the fact that axons are generally longer and less branched than dendrites. To determine whether subtle shape differences might distinguish plus-end-out and minus-end-out branches, we measured length from the first branch point to the tip (Figure 7A, secondary branches, dotted lines) in dendrites in which polarity was defined from movies of EB1-TagRFP-T. We also compared the number of side branches from the main backbone (Figure 7A, orange lines). As fine dendrite tips are difficult to detect using microtubule markers, we made shape measurements using mCD8-GFP. While overall length of plus-end-out and minus-end-out branches was similar, plus-end-out neurites had fewer side branches per length emerging from them (Figure 7B and 7C). Thus, while overall position and patterning of the arbor appeared normal in mosaic arbors, microtubule polarity did affect fine branching.

Discussion

Using Patronin RNAi to generate dendrite arbors with regional differences in microtubule polarity, we compared contents and cytoskeletal organization of plus-end-out and minus-end-out branches. As expected, trafficking of axonal and dendritic cargoes was directed by microtubule polarity, with an axonal cargo accumulating and a dendritic cargo reduced in plus-end-out neurites. We also examined polarized features that might not be expected to be so closely tied to microtubule polarity, including microtubule stability and the ankyrin-based axonal diffusion barrier. We found that microtubules in plus-end-out neurites had stability similar to that in axons, and did not increase dynamics in response to injury like dendritic microtubules. Similarly, we found that ectopic diffusion barriers were associated with mosaic arbors, although their position in the minus-end-out base of the dendrite was unexpected. Shape was surprisingly resistant to alterations in polarity, with only the frequency of side branches differing in plus-end-out and minus-end-out neurites. Overall, the data is consistent with microtubule polarity orchestrating many polarized features of neurons, including microtubule stability and the plasma membrane diffusion barrier, which are themselves important for overall polarity. We therefore favor a model in which microtubule polarity acts at a high level to direct neuronal polarity. One assumption in our interpretation is that reduction of Patronin is primarily affecting polarity. While reduction of Patronin does cause cellular stress in addition to changes in polarity (Feng et al., 2019), this is a global response and would not be expected to differentially affect regions within the same cell. Similarly, minus ends grow similarly in axons and dendrites of dendritic arborization neurons (Feng et al., 2019) and so there is no reason to expect that stability of microtubules would be differently affected in the two compartments by loss of Patronin. Moreover, by comparing regions within the same cell, we should normalize the influence of global changes in microtubule behavior. Thus, although difficult to completely rule out effects of Patronin other than polarity changes, polarity seems most likely to drive differences between neurites in the same dendrite arbor.

One intriguing aspect of the Patronin phenotype is the generation of processes with different polarity, minus-end-out, mixed and plus-end-out, in the same cell. This phenotype is quite different from polarity changes when local nucleation is reduced (Nguyen et al., 2014; Weiner et al., 2020) or when plus end steering through branch points is disrupted (Mattie et al., 2010), both of which result in mixed polarity in dendritic arborization neuron dendrites. Although some dendrite branches are mixed when Patronin is reduced, indicating a failure to establish uniform polarity, other dendrites can organize uniform polarity microtubule arrays, but not always in the correct orientation. During normal development, dendritic arborization neurons have a transient plus-end-out phase when they are very short (Feng et al., 2019). As minus ends grow into dendrites, polarity becomes mixed (Feng et al., 2019). Over several days the number of minus-end-out microtubules gradually increases and polarity resolves to close to uniform minus-end-out (Hill et al., 2012). This resolution step likely involves kinesin-2-mediated steering (Mattie et al., 2010; Weiner et al., 2016) acting as a positive feedback loop to reinforce the dominant polarity. We hypothesize that during development of dendrites with reduced Patronin, some minus ends grow outwards into dendrites. Above a threshold level, positive feedback loops can resolve this to minus-end-out

over time. However, in neurites where the number of minus-end-out microtubules is below a threshold, positive feedback loops will instead generate plus-end-out dendrite branches. Mixed polarity branches could be generated between these two threshold points, or could represent regions that are in the process of resolving to plus-end-out or minus-end-out. It is not clear what drives the segment adjacent to the cell body to be consistently minus-end-out, even when more distal regions have taken on axonal features. This proximal minus-end-out region poses a challenge to axonal cargoes like ANF-GFP that must navigate it to reach the plus-end-out dendrite branches. We have not tracked individual vesicles to determine how they traverse the segment, but the problem is conceptually similar to transport from the cell body to dendrites in Drosophila unipolar neurons. These cells have a single process that emerges from the cell body that has plus-end-out microtubule polarity. It gives rise to dendrites that are minus-end-out (Stone et al., 2008). Dendritic cargoes must therefore first traverse a plus-end-out array or microtubules before reaching minus-end-out dendrites. We analyzed movement of one type of cargo in these cells and found that none moved directly from the plus-end-out primary neurite into dendrites. Instead cargoes either paused at the junction or entered dendrites by retrograde transport from the more distal axon (Stone et al., 2008). It would be interesting to perform a similar analysis on transport between regions of opposite polarity in mosaic neurons.

A naturally occurring example of a cell with a dendrite arbor that has two types of polarity is the C. elegans PVD sensory neuron. In this cell, three neurites emerge from the cell body. One extends anteriorly and gives rise to branched menorah shaped sensory endings that innervate the body wall. This neurite has minus-end-out microtubule polarity like Drosophila dendritic arborization sensory endings (Harterink et al., 2018; Liang et al., 2020; Taylor et al., 2015). An axon also emerges from the cell body and has plus-end-out polarity. A posterior dendrite that has a similar branching pattern to the anterior one is also formed and, surprisingly, has plus-end-out polarity (Harterink et al., 2018; Liang et al., 2020; Taylor et al., 2015). While it is clear that dynein acts as an outbound motor only for the anterior dendrite (Chen et al., 2021; Taylor et al., 2015), a comparison of dendritic features between the anterior and posterior dendrites has not been performed. However, the effect of changing minus-end-out dendritic polarity to plus-end-out on cargo distribution has been assayed in several C. elegans neurons. In kinesin-1 mutants, dendrites of some C. elegans neurons reverse polarity and become plus-end-out (Harterink et al., 2018; Yan et al., 2013), likely because kinesin helps transport a microtubule organizing center to the dendrite tip during outgrowth (Liang et al., 2020). Dendrites with reversed polarity aberrantly accumulate presynaptic components and lose dendritic ones (Yan et al., 2013). But whether this switch in microtubule polarity influences microtubule stability or axon initial segment positioning as we show here is unknown.

A simple model for control of microtubule stability downstream of polarity is that microtubule regulators are transported into neurites using polarity-dependent mechanisms. For example, fidgetin may require dynein to be transported into dendrites so that it is ready to sever microtubules in response to injury, explaining why plus-end-out dendrites do not display increased microtubule dynamics in cut off regions of dendrites (Figure 5). Similarly, microtubule stabilizers may require plus-end-out microtubules for outbound transport from the cell body. This model may, of course, be an oversimplification as even

within a compartment microtubules may have different stability based on their polarity (Tas et al., 2017).

It is more difficult to propose a simple model that accounts for a change in diffusion barrier position based on microtubule polarity. Many studies have suggested a close relationship between the axon initial segment (AIS) and microtubules. Indeed, giant forms of Ankyrin G (AnkG), the master regulator of the AIS in mammals, bind EB proteins, and reduction of AnkG leads to mixed microtubule polarity in the proximal axon (Freal et al., 2016). The influence of AnkG on microtubule polarity is through TRIM46, which can be recruited to membranes by AnkG and EB proteins (Freal et al., 2019) and acts to bundle microtubules in a parallel orientation (van Beuningen et al., 2015). Via this pathway, the AIS can act upstream of microtubule polarity, at least in mammalian neurons where TRIM46 is present. The arrival of TRIM46 at the base of a newly forming axon before AnkG and its requirement to make AnkG-positive neurites (van Beuningen et al., 2015) suggests, however, that this simple linear relationship with AnkG acting upstream of TRIM46 is unlikely. Moreover, despite its ability to form parallel plus-end-out bundles of microtubules when overexpressed in non-neuronal cells TRIM46 was not sufficient to generate additional neurites with an AIS in cultured neurons (van Beuningen et al., 2015). However, microtubule stabilization by taxol was sufficient to generate extra neurites with an AIS (van Beuningen et al., 2015) indicating microtubule properties can position the AIS. These studies in mammalian neurons suggest a complex interplay between the AIS and microtubules, and place microtubule stability as a possible upstream master regulator of axon and AIS formation. Our results suggest that in some scenarios microtubule polarity can also be instructive in forming a plasma membrane diffusion barrier. One hypothesis might be that formation of plus-end-out microtubules could recruit TRIM46, which in turn could recruit giant ankyrins similar to the feedback loop proposed in mammals (Freal et al., 2019). However, there are several problems with this model. First, the family of TRIM proteins has undergone a dramatic expansion in the vertebrate lineage (Marin, 2012; Short and Cox, 2006). In Drosophila there is only one TRIM family member that has the microtubule-binding COS box, Trim9, and while it helps align microtubules in parallel, this function has been linked to dendrites rather than the axon (Feng et al., 2021). Second, the ectopic diffusion barriers are positioned proximal to plus-end-out neurites at the minus-end-out base of the branch. Thus, the generation of ectopic diffusion barriers represents an unexpected output of plus-end-out microtubule polarity.

One aspect of neuronal polarity that was surprisingly resistant to polarity change was shape. In cultured mammalian neurons reduction of minus-end-out microtubules by targeting kinesin-6 results in longer and thinner dendrites (Lin et al., 2012; Sharp et al., 1997). In mosaic dendrite arbors in vivo, we observed only a subtle change in branching. One explanation for this resistance to transforming into a clearly recognizable axon is that in vivo extracellular cues constrain shape much more that in vitro. However, C. elegans motor neurons with reversed polarity due to loss of kinesin-1 have longer dendrites than control neurons (Yan et al., 2013), similar to mammalian cultured neurons with aberrant dendrite microtubule polarity. Moreover, when Drosophila sensory neuron axons are severed near the cell body and a dendrite reverses polarity to become a new axon, this is associated with outgrowth (Rao and Rolls, 2017; Stone et al., 2010) suggesting that the environment can

support axonal extension. One difference between axons regenerating from dendrites and regions with plus-end-out dendrites in mosaic neurons is polarity of microtubules at the base of the neurite. In regenerating axons this regions takes on plus-end-out polarity (Stone et al., 2010), while in mosaic arbors it is minus-end-out. Thus, it is possible that the combination of extrinsic cues and a minus-end-out base restricts growth of plus-end-out dendrites in mosaic arbors. Alternately, axon regeneration is associated with transcriptional changes that promote outgrowth even in the absence of the normal axonal environment.

Materials and Methods

Drosophila maintenance and stocks

For all the experiments, Drosophila larvae were raised at 25°C in fly food vials or bottles. One liter of fly food consists of 4.5g agar, 26g of sucrose, 51.7g of dextrose, 15.5g of yeast, 4 ml of propionic acid, 6 ml of 10% tegosept and 85.8g of cornmeal. To generate cohorts of similar aged larvae, embryos were collected in 35mm petri dishes containing fly food (food cap) for 1 day. After 3 days of incubating food caps at 25°C Drosophila larvae were used for experiments. Fly lines used are summarized in the Resources Table. They include: (a) ppk-gal4, UAS-EB1-TagRFP-T on 3 (control) (b) ppk-gal4, UAS-Patronin-RNAi (Bloomington Drosophila Stock Center, BDSC, line 36659), UAS-EB1-TagRFP-T on 3 (mosaic) (c) 477-gal4, UAS-EB1-GFP on 2; UAS-dicer2 on 3 (d) UAS-Patronin-RNAi (BDSC 36659) (e) UAS-γ-Tubulin-37c-RNAi (Vienna Drosophila Resource Center, VDRC, line 25271) (f) UAS-ANF-GFP (g) UAS-YFP-L10 (h) UAS-tdEos-α-Tubulin (i) 477-gal4, UAS-tdEos-α-Tubulin (j) UAS-iBlueberry (k) UAS-mCD8-GFP (see Resources Table). The 477-tester line included UAS-dicer2 to increase knockdown efficiency of long RNA hairpins in neurons (Dietzl et al., 2007).

Construction of mosaic tester line

The UAS-EB1-TagRFP-T line generated in the previous study (Feng et al., 2021) was recombined with ppk-gal4 on chromosome III. The UAS-Patronin-RNAi was further recombined onto III by screening for plus-end-out polarity phenotype in the class IV ddaC neurons. The final genotype of the tester line to generate mosaic neurons was: ppk-gal4, UAS-EB1-TagRFP-T, Patronin-RNAi/TM6.

Live imaging of Drosophila larvae

3-day-old drosophila larvae were mounted with a drop of water onto an agarose pad on the surface of a glass slide that allows immobilization of the larva. A coverslip was placed on the larva and taped to the slide such that the larva is lightly pressed and has the dorsal side facing upwards. The ddaC neurons in the a2 or a3 segment were chosen for imaging for consistency. In all the experiments, only one neuron was imaged from one larva/animal.

All Z-stack images/ time-lapse videos were acquired using a Zeiss LSM800 upright confocal microscope with a Plan-Apochromat 63× 1.4 NA oil objective unless otherwise mentioned. EB1-TagRFP-T movies were 150 frames at one frame per two seconds, so total duration of five minutes. These movies were taken at 0.5x zoom in order to cover most of the dendritic arbor. Time-lapse videos of EB1-GFP were taken with a widefield Zeiss Imager

M2 microscope with AxioCam M2 camera and 63× 1.4 NA Plan-Apochromat oil immersion objective. Zeiss Zen Blue software was used to record 300-frames at the speed of one frame per second, so duration of five minutes. Figure 4F was generated using the AiryScan detector and processing on a Zeiss LSM800 upright microscope.

Microtubule polarity assay

EB1 time-lapse videos were processed as .tif files using FIJI image analysis software (https://imagej.net/software/fiji/)(Schindelin et al., 2012). The template-matching plugin was used to align videos in case the larva moved slightly while imaging. The bleach correction tool was used for movies with EB1-GFP. The number of comets moving towards the cell body (minus-end-out) or away from the cell body (plus-end-out) were counted manually and confirmed by generating kymographs using the multi-kymograph plugin in the FIJI-image analysis software. Only fast-moving plus end comets that were present at least for three consecutive frames were included in the quantification. Neurites with 90% or more plus-end-out microtubules were categorized as plus-end-out, neurites with over 90% minus-end-out microtubules were categorized as minus-end-out, and all the intermediates were categorized as mixed.

Imaging of axon/dendrite-specific cargo

A Drosophila line containing a tagged neuropeptide, UAS-ANF-GFP (Wong et al., 2012) line was crossed with the mosaic tester line and Z stacks of GFP were acquired as were EB1-TagRFP-T movies. YFP-L10 (Rolls et al., 2007) localization in mosaic neurons was assessed using a similar strategy. Z stacks were processed to generate maximum-intensity projections using FIJI. For each neuron imaged, the corresponding EB-video was used to map the microtubule polarity of each neurite. The neurites were categorized according to the method described in the microtubule polarity assay.

The presence of ANF-GFP puncta was checked in neurite regions as indicated in the example images. The segmented line tool was used to trace the neurite and the ANF-GFP fluorescence in the form of line profile was studied. If there were any distinct peaks, the neurite was scored as positive for ANF-GFP.

For measuring YFP-L10 intensity at the branchpoints, a region of interest to outline the branchpoint was drawn with the polygon selection tool in FIJI. The average fluorescence intensity (F.I) of the branchpoint was recorded in this region. F.I was quantified from branch points that had the same polarity in the segments preceding and following the branchpoint.

EB1 dynamics quantitation

From time-lapse videos acquired as described above, the number of EB1 comets was quantified from neurites in focus. For each movie the entire five minute acquisition was scored. Kymographs generated using the multi-kymograph tool in FIJI and direct analysis of videos were cross-checked to make sure each comet was counted once. The length of the neurite in focus was also recorded in order to normalize the EB1 dynamics with length. The segmented-line tool in the FIJI imaging software was used to measure the length of the

neurite. In addition to counting total numbers of comets in a neurite, the direction of comet movement was scored to assign polarity.

Measurement of tubulin intensity to normalize EB1 dynamics

UAS-tdEos-α–Tubulin transgenic flies (Lu et al., 2013) were crossed to the mosaic tester line and their Z-stack images were taken to measure the intensity of tdEos-α-Tubulin. The tiling feature in the LSM800 was used for this assay. The tiled images were processed as .tif files and maximum intensity projections were generated. The segmented line tool was used to measure average fluorescence intensity of the neurite. Microtubule polarity of the corresponding neurite was assessed using EB1 time-lapse videos. The number of EB1-comets recorded per 10μm dendrite was further divided by the corresponding tubulin intensity for normalization.

Microtubule dynamics before and after neurite severing

Before injury time-lapse videos of EB1-GFP were acquired for a duration of 90 frames at one frame per second. Then a single neurite was severed using a MicroPoint pulsed UV laser (Andor Technology). Animals were recovered to normal media and incubated for one hour at room temperature. One hour after injury, animals were remounted on slides and time-lapse videos of EB1-GFP were recorded 200 to 300 frames at one frame per second. The number of EB1 comets in neurites was counted and normalized to duration of the time-lapse and length of the neurite. Time-lapse videos were acquired using a Zeiss Imager M2 microscope equipped with Zen Blue software, an AxioCam M2 camera and a 63× 1.4 NA Plan-Apochromat oil immersion objective. To compare the effects of injury on axons and dendrites in control neurons and plus-end-out and minus-end-out regions of mosaic neurons we binned outcomes into two categories: 1- increase in microtubule dynamics and 2- no increase in microtubule dynamics. We then used a Fisher's exact test to compare control dendrites and axons and plus-end-out and minus-end-out regions of mosaic arbors.

Neuronal morphology

Flies containing a UAS-mCD8-GFP transgene were crossed with flies from the mosaic tester line to visualize the morphology of the neuron. The tiling feature of the Zeiss LSM800 confocal microscope was used to acquire Z stack images. Maximum intensity projections were generated using FIJI. For each neuron imaged, a corresponding EB video was recorded to map the microtubule polarity of each neurite. Neurites were categorized as described in the microtubule polarity assay section. The length of secondary neurites was quantified using the segmented-line tool on FIJI. The number of terminal branches was counted manually and normalized to the length of the neurite.

Fluorescence recovery after photobleaching (FRAP) to test the presence of diffusion barrier

The photobleaching assay was similar to that used in our previous work on the axon initial segment in Drosophila neurons (Jegla et al., 2016b). Time-lapse movies were recorded on an LSM800 microscope. A 5-micron region was bleached either adjacent to the cell body or at the base of the plus-end-out part of a dendrite. Time-lapse

movies were processed and analyzed to generate fractional recovery curves using FIJI and normalized with the unbleached region using FRAP calculator in FIJI developed by Dr. Robert Bagnell (https://www.med.unc.edu/microscopy/resources/imagej-plugins-and-macros/frap-calculator-macro/).

Supplementary Material

Refer to Web version on PubMed Central for supplementary material.

Acknowledgements

References

Baas PW, Deitch JS, Black MM **and** Banker GA (1988). Polarity orientation of microtubules in hippocampal neurons: uniformity in the axon and nonuniformity in the dendrite. Proc Natl Acad Sci U S A 85, 8335–9. [PubMed: 3054884] **and**

Baas PW **and** Lin S (2011). Hooks and comets: The story of microtubule polarity orientation in the neuron. Dev Neurobiol 71, 403–18. [PubMed: 21557497] **and**

Baas PW, Rao AN, Matamoros AJ **and** Leo L (2016). Stability properties of neuronal microtubules. Cytoskeleton (Hoboken) 73, 442–60. [PubMed: 26887570] **and**

Baas PW, Slaughter T, Brown A **and** Black MM (1991). Microtubule dynamics in axons and dendrites. J Neurosci Res 30, 134–53. [PubMed: 1795398] **and**

Bartlett WP **and** Banker GA (1984). An electron microscopic study of the development of axons and dendrites by hippocampal neurons in culture. I. Cells which develop without intercellular contacts. J Neurosci 4, 1944–53. [PubMed: 6470762] **and**

Chen YC, Huang HR, Hsu CH **and** Ou CY (2021). CRMP/UNC-33 organizes microtubule bundles for KIF5-mediated mitochondrial distribution to axon. PLoS Genet 17, e1009360. [PubMed: 33571181] **and**

Craig AM **and** Banker G (1994). Neuronal polarity. Annu Rev Neurosci 17, 267–310. [PubMed: 8210176] **and**

Dietzl G, Chen D, Schnorrer F, Su KC, Barinova Y, Fellner M, Gasser B, Kinsey K, Oppel S, Scheiblauer S et al. (2007). A genome-wide transgenic RNAi library for conditional gene inactivation in Drosophila. Nature 448, 151–6. [PubMed: 17625558]

Feng C, Cleary JM, Kothe GO, Stone MC, Weiner AT, Hertzler JI, Hancock WO **and** Rolls MM (2021). Trim9 and Klp61F promote polymerization of new dendritic microtubules along parallel microtubules. J Cell Sci 134.**and**

Feng C, Thyagarajan P, Shorey M, Seebold DY, Weiner AT, Albertson RM, Rao KS, Sagasti A, Goetschius DJ **and** Rolls MM (2019). Patronin-mediated minus end growth is required for dendritic microtubule polarity. J Cell Biol 218, 2309–2328. [PubMed: 31076454] **and**

Freal A, Fassier C, Le Bras B, Bullier E, De Gois S, Hazan J, Hoogenraad CC **and** Couraud F (2016). Cooperative Interactions between 480 kDa Ankyrin-G and EB Proteins Assemble the Axon Initial Segment. J Neurosci 36, 4421–33. [PubMed: 27098687] **and**

Freal A, Rai D, Tas RP, Pan X, Katrukha EA, van de Willige D, Stucchi R, Aher A, Yang C, Altelaar AFM et al. (2019). Feedback-Driven Assembly of the Axon Initial Segment. Neuron 104, 305–321 e8. [PubMed: 31474508]

Goodwin PR, Sasaki JM **and** Juo P (2012). Cyclin-dependent kinase 5 regulates the polarized trafficking of neuropeptide-containing dense-core vesicles in Caenorhabditis elegans motor neurons. J Neurosci 32, 8158–72. [PubMed: 22699897] **and**

Goodwin SS **and** Vale RD (2010). Patronin regulates the microtubule network by protecting microtubule minus ends. Cell 143, 263–74. [PubMed: 20946984] **and**

Grueber WB, Jan LY **and** Jan YN (2002). Tiling of the Drosophila epidermis by multidendritic sensory neurons. Development 129, 2867–78. [PubMed: 12050135] **and**

Hammond JW, Huang CF, Kaech S, Jacobson C, Banker G **and** Verhey KJ (2010). Posttranslational modifications of tubulin and the polarized transport of kinesin-1 in neurons. Mol Biol Cell 21, 572–83. [PubMed: 20032309] **and**

Harterink M, Edwards SL, de Haan B, Yau KW, van den Heuvel S, Kapitein LC, Miller KG **and** Hoogenraad CC (2018). Local microtubule organization promotes cargo transport in C. elegans dendrites. J Cell Sci**and**

Hedstrom KL, Ogawa Y **and** Rasband MN (2008). AnkyrinG is required for maintenance of the axon initial segment and neuronal polarity. J Cell Biol 183, 635–40. [PubMed: 19001126] **and**

Hendershott MC **and** Vale RD (2014). Regulation of microtubule minus-end dynamics by CAMSAPs and Patronin. Proc Natl Acad Sci U S A 111, 5860–5. [PubMed: 24706919] **and**

Hertzler JI, Simonovitch SI, Albertson RM, Weiner AT, Nye DMR **and** Rolls MM (2020). Kinetochore proteins suppress neuronal microtubule dynamics and promote dendrite regeneration. Mol Biol Cell 31, 2125–2138. [PubMed: 32673176] **and**

Hill SE, Parmar M, Gheres KW, Guignet MA, Huang Y, Jackson FR **and** Rolls MM (2012). Development of dendrite polarity in Drosophila neurons. Neural Dev 7, 34. [PubMed: 23111238] **and**

Horton AC, Racz B, Monson EE, Lin AL, Weinberg RJ **and** Ehlers MD (2005). Polarized secretory trafficking directs cargo for asymmetric dendrite growth and morphogenesis. Neuron 48, 757–71. [PubMed: 16337914] **and**

Hwang RY, Zhong L, Xu Y, Johnson T, Zhang F, Deisseroth K **and** Tracey WD (2007). Nociceptive neurons protect Drosophila larvae from parasitoid wasps. Curr Biol 17, 2105–16. [PubMed: 18060782] **and**

Jegla T, Nguyen MM, Feng C, Goetschius DJ, Luna E, van Rossum DB, Kamel B, Pisupati A, Milner ES **and** Rolls MM (2016a). Bilaterian Giant Ankyrins Have a Common Evolutionary Origin and Play a Conserved Role in Patterning the Axon Initial Segment. PLoS Genet 12, e1006457. [PubMed: 27911898] **and**

Jegla T, Nguyen MM, Feng C, Goetschius DJ, Luna E, van Rossum DB, Kamel B, Pisupati A, Milner ES **and** Rolls MM (2016b). Bilaterian Giant Ankyrins Have a Common Evolutionary Origin and Play a Conserved Role in Patterning the Axon Initial Segment. PLOS Genetics 12, e1006457–e1006457. [PubMed: 27911898] **and**

Jenkins PM, Kim N, Jones SL, Tseng WC, Svitkina TM, Yin HH **and** Bennett V (2015). Giant ankyrin-G: a critical innovation in vertebrate evolution of fast and integrated neuronal signaling. Proc Natl Acad Sci U S A 112, 957–64. [PubMed: 25552556] **and**

Jiang K, Hua S, Mohan R, Grigoriev I, Yau KW, Liu Q, Katrukha EA, Altelaar AF, Heck AJ, Hoogenraad CC et al. (2014). Microtubule minus-end stabilization by polymerization-driven CAMSAP deposition. Dev Cell 28, 295–309. [PubMed: 24486153]

Kollins KM, Bell RL, Butts M **and** Withers GS (2009). Dendrites differ from axons in patterns of microtubule stability and polymerization during development. Neural Dev 4, 26. [PubMed: 19602271] **and**

Liang X, Kokes M, Fetter RD, Sallee MD, Moore AW, Feldman JL **and** Shen K (2020). Growth cone-localized microtubule organizing center establishes microtubule orientation in dendrites. Elife 9.**and**

Lin S, Liu M, Mozgova OI, Yu W **and** Baas PW (2012). Mitotic motors coregulate microtubule patterns in axons and dendrites. J Neurosci 32, 14033–49. [PubMed: 23035110] **and**

Lu W, Fox P, Lakonishok M, Davidson MW **and** Gelfand VI (2013). Initial neurite outgrowth in Drosophila neurons is driven by Kinesin-powered microtubule sliding. Curr Biol 23, 1018–23. [PubMed: 23707427] **and**

Marin I (2012). Origin and diversification of TRIM ubiquitin ligases. PLoS One 7, e50030. [PubMed: 23185523]

Mattie FJ, Stackpole MM, Stone MC, Clippard JR, Rudnick DA, Qiu Y, Tao J, Allender DL, Parmar M **and** Rolls MM (2010). Directed Microtubule Growth, +TIPs, and Kinesin-2 Are Required for Uniform Microtubule Polarity in Dendrites. Curr Biol 20, 2169–77. [PubMed: 21145742] **and**

Nakada C, Ritchie K, Oba Y, Nakamura M, Hotta Y, Iino R, Kasai RS, Yamaguchi K, Fujiwara T **and** Kusumi A (2003). Accumulation of anchored proteins forms membrane diffusion barriers during neuronal polarization. Nat Cell Biol 5, 626–32. [PubMed: 12819789] **and**

Nguyen MM, McCracken CJ, Milner ES, Goetschius DJ, Weiner AT, Long MK, Michael NL, Munro S **and** Rolls MM (2014). Gamma-tubulin controls neuronal microtubule polarity independently of Golgi outposts. Mol Biol Cell 25, 2039–50. [PubMed: 24807906] **and**

Ori-McKenney KM, Jan LY **and** Jan YN (2012). Golgi outposts shape dendrite morphology by functioning as sites of acentrosomal microtubule nucleation in neurons. Neuron 76, 921–30. [PubMed: 23217741] **and**

Rao KS **and** Rolls MM (2017). Two Drosophila model neurons can regenerate axons from the stump or from a converted dendrite, with feedback between the two sites. Neural Development 12.**and**

Rasband MN (2010). The axon initial segment and the maintenance of neuronal polarity. Nat Rev Neurosci

Rolls MM **and** Jegla TJ (2015). Neuronal polarity: an evolutionary perspective. J Exp Biol 218, 572–80. [PubMed: 25696820] **and**

Rolls MM, Satoh D, Clyne PJ, Henner AL, Uemura T **and** Doe CQ (2007). Polarity and compartmentalization of Drosophila neurons. Neural Development 2, 7. [PubMed: 17470283] **and**

Rolls MM, Thyagarajan P **and** Feng C (2020). Microtubule dynamics in healthy and injured neurons. Dev Neurobiol**and**

Schindelin J, Arganda-Carreras I, Frise E, Kaynig V, Longair M, Pietzsch T, Preibisch S, Rueden C, Saalfeld S, Schmid B et al. (2012). Fiji: an open-source platform for biological-image analysis. Nat Methods 9, 676–82. [PubMed: 22743772]

Sharp DJ, Yu W, Ferhat L, Kuriyama R, Rueger DC **and** Baas PW (1997). Identification of a microtubule-associated motor protein essential for dendritic differentiation. J Cell Biol 138, 833–43. [PubMed: 9265650] **and**

Short KM **and** Cox TC (2006). Subclassification of the RBCC/TRIM superfamily reveals a novel motif necessary for microtubule binding. J Biol Chem 281, 8970–80. [PubMed: 16434393] **and**

Song AH, Wang D, Chen G, Li Y, Luo J, Duan S **and** Poo MM (2009). A selective filter for cytoplasmic transport at the axon initial segment. Cell 136, 1148–60. [PubMed: 19268344] **and**

Stepanova T, Slemmer J, Hoogenraad CC, Lansbergen G, Dortland B, De Zeeuw CI, Grosveld F, van Cappellen G, Akhmanova A **and** Galjart N (2003). Visualization of microtubule growth in cultured neurons via the use of EB3-GFP (end-binding protein 3-green fluorescent protein). J Neurosci 23, 2655–64. [PubMed: 12684451] **and**

Stone MC, Nguyen MM, Tao J, Allender DL **and** Rolls MM (2010). Global up-regulation of microtubule dynamics and polarity reversal during regeneration of an axon from a dendrite. Mol Biol Cell 21, 767–77. [PubMed: 20053676] **and**

Stone MC, Roegiers F **and** Rolls MM (2008). Microtubules Have Opposite Orientation in Axons and Dendrites of Drosophila Neurons. Mol Biol Cell 19, 4122–9. [PubMed: 18667536] **and**

Tao J, Feng C **and** Rolls MM (2016). The microtubule-severing protein fidgetin acts after dendrite injury to promote their degeneration. J Cell Sci 129, 3274–81. [PubMed: 27411367] **and**

Tas RP, Chazeau A, Cloin BMC, Lambers MLA, Hoogenraad CC **and** Kapitein LC (2017). Differentiation between Oppositely Oriented Microtubules Controls Polarized Neuronal Transport. Neuron 96, 1264–1271 e5. [PubMed: 29198755] **and**

Taylor CA, Yan J, Howell AS, Dong X **and** Shen K (2015). RAB-10 Regulates Dendritic Branching by Balancing Dendritic Transport. PLoS Genet 11, e1005695. [PubMed: 26633194] **and**

van Beuningen SF **and** Hoogenraad CC (2016). Neuronal polarity: remodeling microtubule organization. Curr Opin Neurobiol 39, 1–7. [PubMed: 26945466] **and**

van Beuningen SFB, Will L, Harterink M, Chazeau A, van Battum EY, Frias CP, Franker MAM, Katrukha EA, Stucchi R, Vocking K et al. (2015). TRIM46 Controls Neuronal Polarity and Axon

Author Manuscript Author Manuscript Author Manuscript Author Manuscript

Specification by Driving the Formation of Parallel Microtubule Arrays. Neuron 88, 1208–1226. [PubMed: 26671463]

Wang Y, Rui M, Tang Q, Bu S **and** Yu F (2019). Patronin governs minus-end-out orientation of dendritic microtubules to promote dendrite pruning in Drosophila. Elife 8.**and**

Weiner AT, Lanz MC, Goetschius DJ, Hancock WO **and** Rolls MM (2016). Kinesin-2 and Apc function at dendrite branch points to resolve microtubule collisions. Cytoskeleton (Hoboken) 73, 35–44. [PubMed: 26785384] **and**

Weiner AT, Seebold DY, Torres-Gutierrez P, Folker C, Swope RD, Kothe GO, Stoltz JG, Zalenski MK, Kozlowski C, Barbera DJ et al. (2020). Endosomal Wnt signaling proteins control microtubule nucleation in dendrites. PLoS Biol 18, e3000647. [PubMed: 32163403]

Wiese C (2008). Distinct Dgrip84 isoforms correlate with distinct gamma-tubulins in Drosophila. Mol Biol Cell 19, 368–77. [PubMed: 18003974]

Winckler B, Forscher P **and** Mellman I (1999). A diffusion barrier maintains distribution of membrane proteins in polarized neurons. Nature 397, 698–701. [PubMed: 10067893] **and**

Witte H, Neukirchen D **and** Bradke F (2008). Microtubule stabilization specifies initial neuronal polarization. J Cell Biol 180, 619–32. [PubMed: 18268107] **and**

Wong MY, Zhou C, Shakiryanova D, Lloyd TE, Deitcher DL **and** Levitan ES (2012). Neuropeptide delivery to synapses by long-range vesicle circulation and sporadic capture. Cell 148, 1029–38. [PubMed: 22385966] **and**

Yan J, Chao DL, Toba S, Koyasako K, Yasunaga T, Hirotsune S **and** Shen K (2013). Kinesin-1 regulates dendrite microtubule polarity in Caenorhabditis elegans. Elife 2, e00133. [PubMed: 23482306] **and**

Yau KW, Schatzle P, Tortosa E, Pages S, Holtmaat A, Kapitein LC **and** Hoogenraad CC (2016). Dendrites In Vitro and In Vivo Contain Microtubules of Opposite Polarity and Axon Formation Correlates with Uniform Plus-End-Out Microtubule Orientation. J Neurosci 36, 1071–85. [PubMed: 26818498] **and**

Ye B, Zhang Y, Song W, Younger SH, Jan LY **and** Jan YN (2007). Growing dendrites and axons differ in their reliance on the secretory pathway. Cell 130, 717–29. [PubMed: 17719548] **and**

Yu D, Dong Z, Gustafson WC, Ruiz-Gonzalez R, Signor L, Marzocca F, Borel F, Klassen MP, Makhijani K, Royant A et al. (2016). Rational design of a monomeric and photostable far-red fluorescent protein for fluorescence imaging in vivo. Protein Sci 25, 308–15. [PubMed: 26549191]

Yu W, Cook C, Sauter C, Kuriyama R, Kaplan PL **and** Baas PW (2000). Depletion of a microtubule-associated motor protein induces the loss of dendritic identity. J Neurosci 20, 5782–91. [PubMed: 10908619] **and**

Highlights

Mosaic dendrites with regionally distinct microtubule polarity were used as a model

Microtubule polarity directed axon and dendrite cargo to different dendrite branches

Plus-end-out dendrites had more stable microtubules than minus-end-out ones

Ectopic diffusion barriers were formed at the base of plus-end-out dendrites

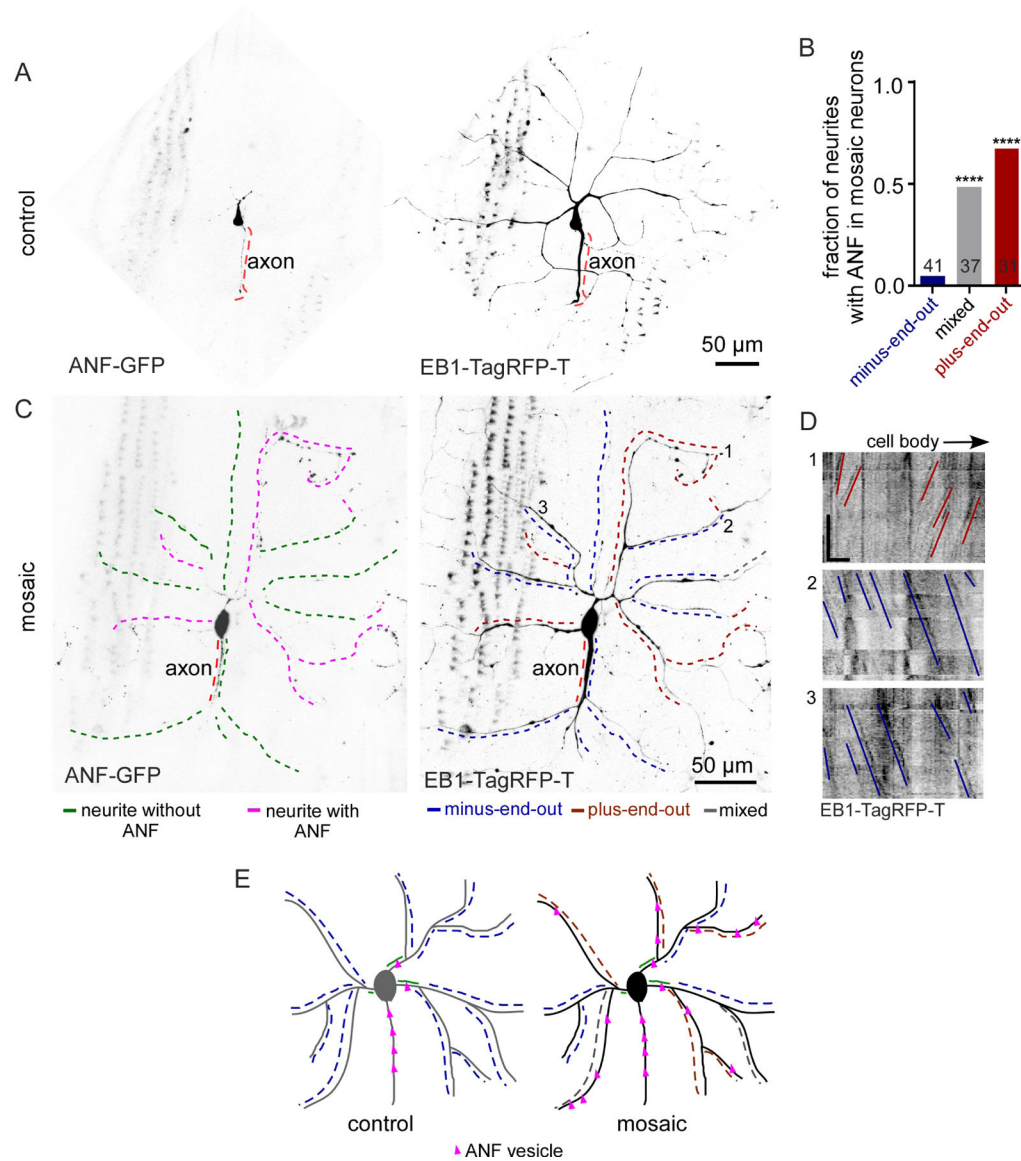Fewer side branches were present in plus-end-out dendrite branches

Figure 1. Reduction of Patronin generates mosaic dendrite arbors with plus-end-out and minus-end-out regions emerging from minus-end-out roots.

A. Representative image of a class IV ddaC (dorsal dendrite arborization-C) neuron expressing UAS-EB1-GFP and UAS-Patronin RNAi under 477-Gal4 in a 3-day-old Drosophila larva. The black dotted line labels the axon. The red and blue dashed lines indicate the regions of neurites/dendritic branches with plus-end-out microtubules and minus-end-out microtubules respectively. The grey dotted lines mark neurites with mixed microtubule polarity. The green solid line marks the base of a dendrite.

B. Representative kymographs of EB1-GFP controlled by 477-Gal4 from time-lapse videos of neurites from control and mosaic (Patronin RNAi) dendrite arbors. γ-Tubulin-37c-RNAi was used as the control RNAi – this gene is maternally expressed and does not contribute to somatic function (Wiese, 2008). Blue lines mark the minus-end-out microtubules while red lines mark the plus-end-out microtubules. Scale bar: x axis = 5 μm, y axis = 60 seconds.

C. Quantification of dendritic branches expressing EB1-GFP under 477-gal4 displaying different microtubule polarities: plus-end-out microtubules (>90%), minus-end-out microtubules (>90%) and mixed polarity. Numbers on the graphs are the total number of branches collected for each group from 15 animals.

D. Representative kymograph from time-lapse video of a segment from the base of the mosaic dendrite arbor where the blue lines label minus-end-out microtubules. Quantification of polarity of microtubules in the base of the control and mosaic arbors is shown in the graph. Numbers on the graphs are the total number of branches collected from 12 animals.

E. Representative image of a class IV ddaC neuron expressing EB1-TagRFP-T and Patronin RNAi under ppk-gal4 in a 3-day-old Drosophila larva. The black dotted line labels the axon. Red and blue dashed lines mark the neurites/dendritic branches with plus-end-out microtubules and minus-end-out microtubules respectively.

F. Representative kymographs from time-lapse videos of a segment of neurites expressing EB1-TagRFP-T under ppk-gal4 from mosaic dendrite arbors are shown. Blue lines mark minus-end-out microtubules while red lines mark plus-end-out microtubules. Scale bar: x axis = 10 μm, y axis = 60 seconds.

G. Schematic diagrams of control and mosaic (Patronin RNAi) neurons are shown.

H. The fraction of dendritic branches with different microtubule polarity in individual neurons (same color code as in C) are compared between 477-gal4 and ppk-gal4. The distribution in each neuron is plotted in the graphs.
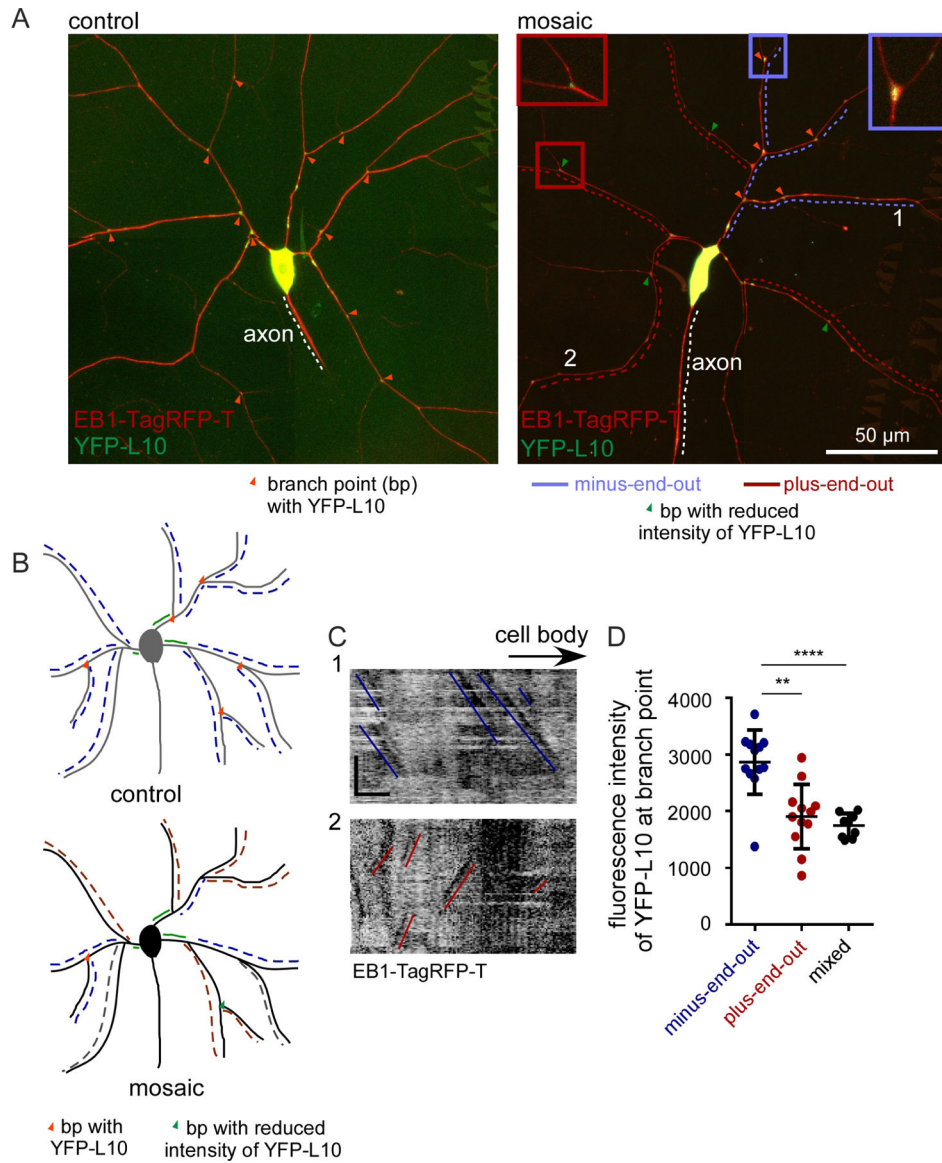
Figure 2. Axonal cargo is routed to plus-end-out dendrites.

A. Representative images of Class 4 ddaC neurons expressing ANF-GFP (axonal marker) and EB1-Tag-RFP-T in control neurons are shown.

B. Quantification of microtubule polarity and ANF-GFP localization in mosaic neurons. ****, P<0.0001 when analyzed with student's t-test. The numbers on the graph represent the total number of neurites quantified from 16 animals.

C. Representative images of mosaic class IV ddaC neurons expressing ANF-GFP and EB1-Tag-RFP-T. Note that in this example the axon (red dashed line) is under one of the dendrites. In the left panel, pink dashed lines indicate neurites with distinct ANF puncta while green dashed lines indicate neurites without ANF. Microtubule polarity (from time-lapse video of EB-dynamics) in these neurites is mapped in the right panel as red lines for plus-end-out, blue lines for minus-end-out and grey lines for mixed.

D. Kymographs of a segment of the regions marked with numbers in B (from time-lapsed video of EB-comets) showing different microtubule polarity. Red lines mark plus-end-out microtubules while the blue lines mark the minus-end-out microtubules. Scale bar, x axis = 10 μm, y axis = 60 seconds.

E. Schematic diagram showing localization of ANF-GFP in control and mosaic neurons. The color code of microtubule polarity is as described in 1G. Pink triangles represent ANF puncta.
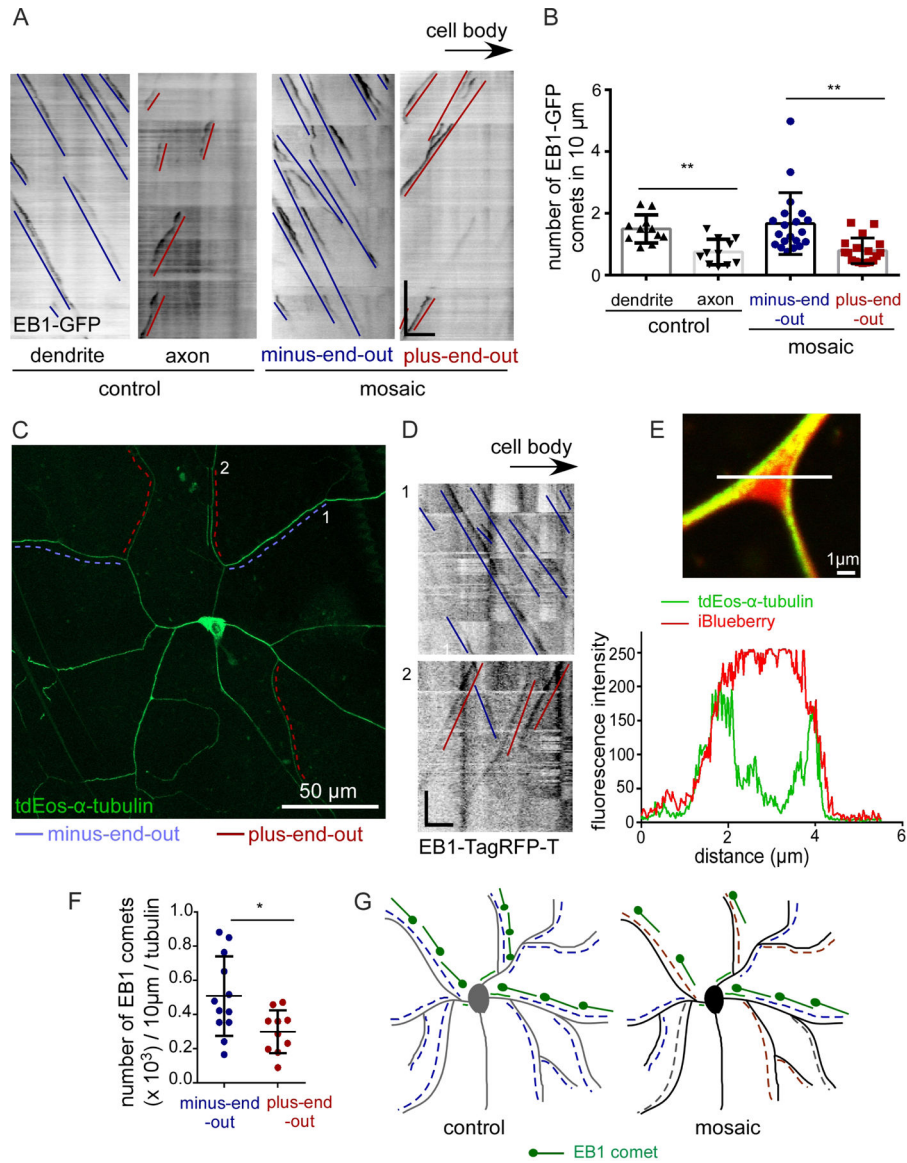
Figure 3. Ribosome localization is reduced in plus-end-out neurites.

A. Representative images of ddaC control and mosaic neuron expressing the dendrite-specific ribosomal marker YFP-L10. Orange arrowheads mark branch points with YFP-L10 localization. Insets show zoomed-in branchpoint regions with minus-end-out polarity (in blue) and plus-end-out polarity (in red).

B. Schematic diagram showing YFP-L10 distribution in branch points (bp) of control and mosaic neurons.

C. Kymographs from regions marked with numbers in A showing microtubule polarity in mosaic neurons expressing YFP-L10. Red lines mark plus-end-out microtubules while the blue lines mark minus-end-out microtubules. Scale bar, x axis = 10 μm, y axis = 60 seconds.

D. Quantification of fluorescence intensity of YFP-L10 at branch points. Branch points were were selected for quantitation only if regions on either side had the same polarity. **, P<0.01 when analyzed with student's t-test. Branch points were quantified from 11 mosaic neurons.
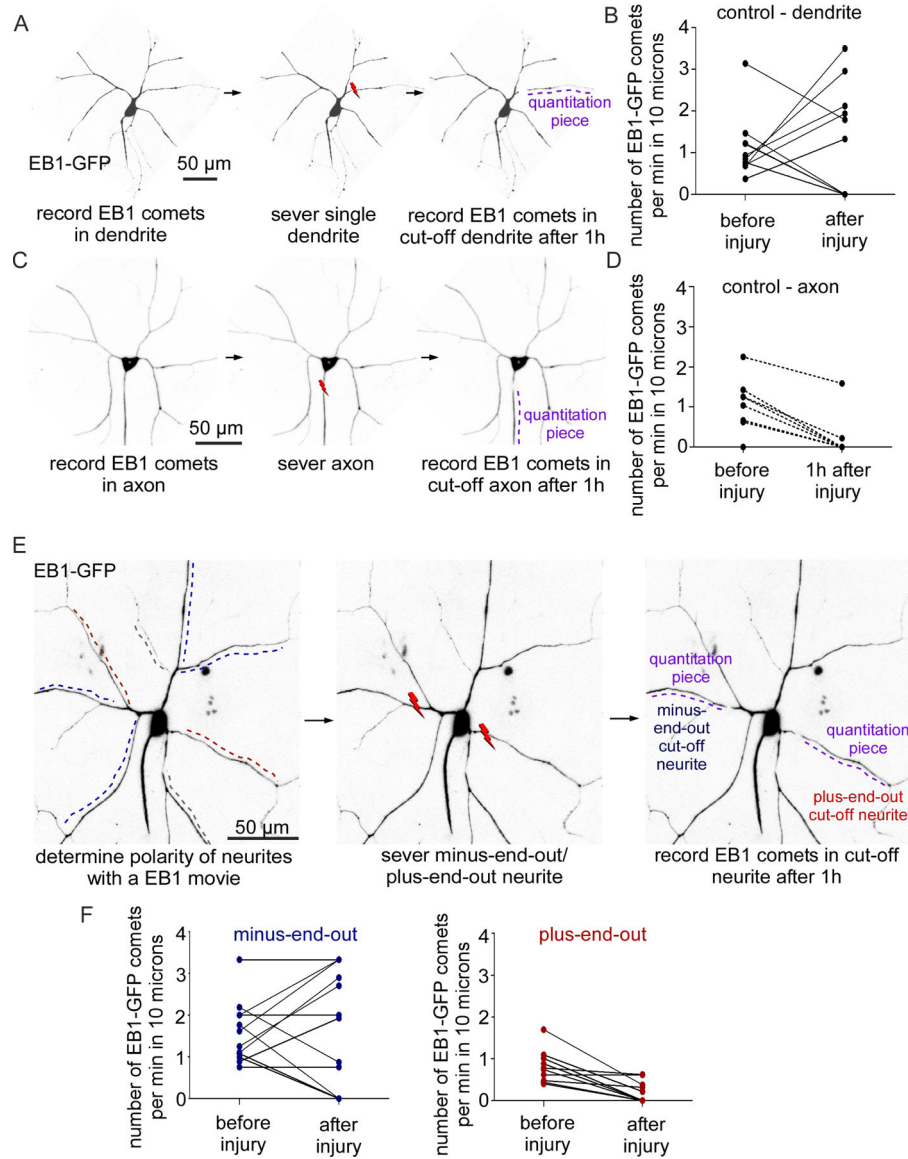
Figure 4. Microtubule stability differs in plus-end-out and minus-end-out neurites of mosaic arbors.

A. Representative kymographs showing EB1-GFP dynamics in a control dendrite and axon and in minus-end-out and plus-end-out regions of mosaic arbors. Minus-end-out microtubules are labelled with blue lines while red lines label plus-end-out microtubules. Scale bar: x axis = 5 μm, y axis = 60 seconds.

B. Quantification of EB1-GFP dynamics in control neurons (n=10 animals) and mosaic dendrite arbors (n=15 animals). **, P<0.01 when analyzed with student's t-test.

C. Representative image of a ddaC neuron expressing tdEos-α-Tubulin. Microtubule polarity is indicated with red lines for plus-end-out and blue lines for minus-end-out.

D. Kymographs of the regions marked with numbers in C (from time-lapse videos of EB1-TagRFP-T comets) showing different microtubule polarity. Red lines mark plus-end-out microtubules while blue lines mark minus-end-out microtubules. Scale bar, x axis = 10 μm, y axis = 60 seconds.

E. Airyscan image of branch point of a ddaC neuron expressing tdEos-α-Tubulin and iBlueberry (soluble marker). Fluorescence intensity was measured along the white line through the branch point and is shown in the graph.

F. Quantification of EB1-TagRFP-T dynamics after normalization to tdEos-α-Tubulin intensity in a neurite (n=10 animals). *, P<0.05.

G. Schematic diagram shows plus end (EB1 comet) number is similar in control and minus-end-out regions of mosaic dendrites, but reduced in plus-end-out regions.
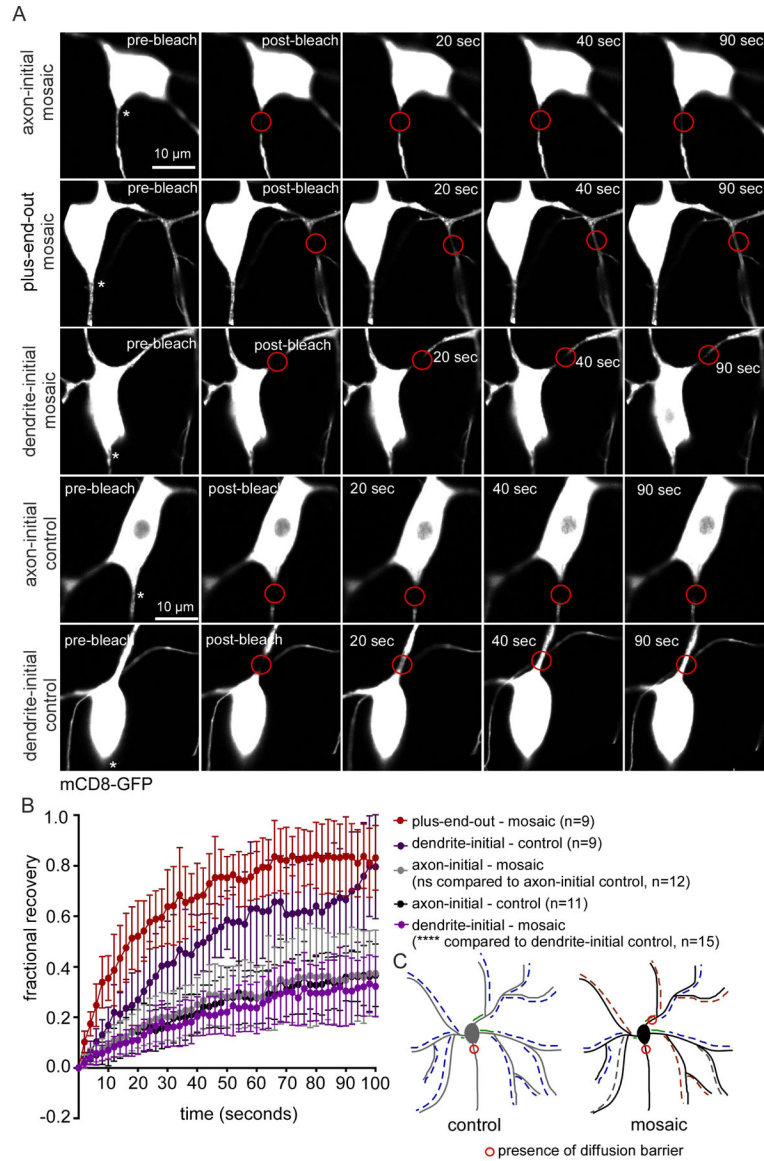
Figure 5. Microtubules in minus-end-out, but not plus-end-out, regions of mosaic arbors show the dendritic response to neurite severing.

A. Schematics showing the dendrite injury assay for control neurons. Lightning bolt indicates site of severing.

B. Quantification of EB1-GFP dynamics before and after dendrite injury in control neurons, n = 10 animals.

C. Schematics showing axon injury assay in control neurons.

D. Quantification of EB1-dynamics before and after axon injury in control neurons, n = 10 animals. P<0.05 when the outcomes (increase in comet number vs no increase) were compared using the Fisher's Exact test between 5B and 5D.

E. Schematics showing the assay to measure EB1-GFP dynamics after injury in mosaic ddaC neurons. Plus-end-out neurites are marked with red lines and minus-end-out with blue lines.

F. Quantification of EB1-GFP dynamics before and after injury in mosaic neurons (n = 16 animals). P<0.05 when the outcomes (increase in comet number vs no increase) were compared using the Fisher's Exact test between minus-end-out and plus-end-out neurites.
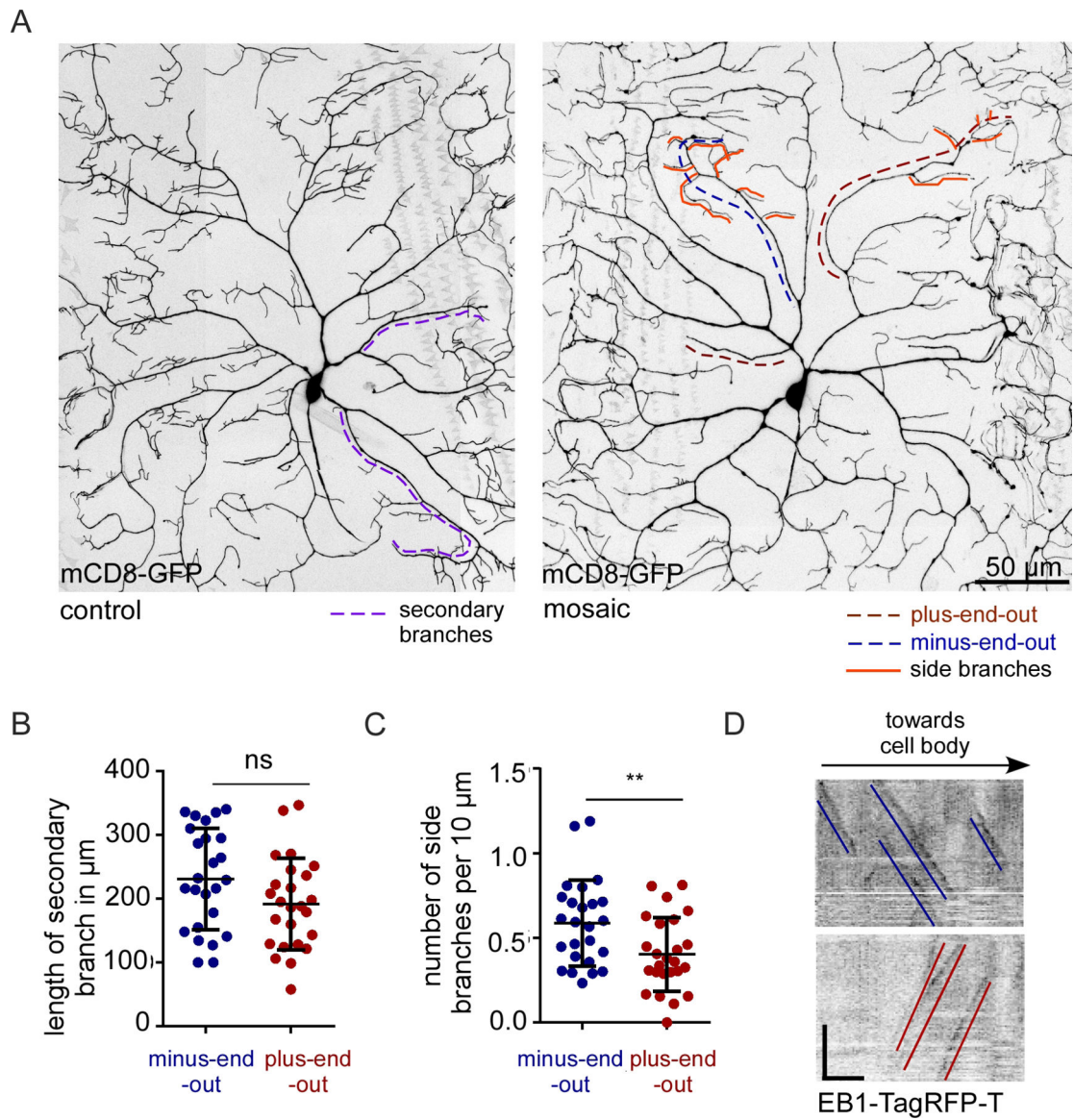
Figure 6. Ectopic diffusion barriers form in neurons with mosaic arbors.

A. Representative images of neurons expressing mCD8-GFP (membrane marker) at different time points from the time-lapse movie recorded during photobleaching assays. In all images the axons emerge from the bottom of the cell body and are indicated with asterisks. Red circles mark the bleached region.

B. Quantification of fluorescence recovery after photobleaching (FRAP). Error bars show the standard deviation. The average intensity values between 80 and 100 seconds post-bleaching of the specified categories were compared with a student's t-test.

C. Schematic diagram showing the location of diffusion barriers in the control and mosaic neurons.
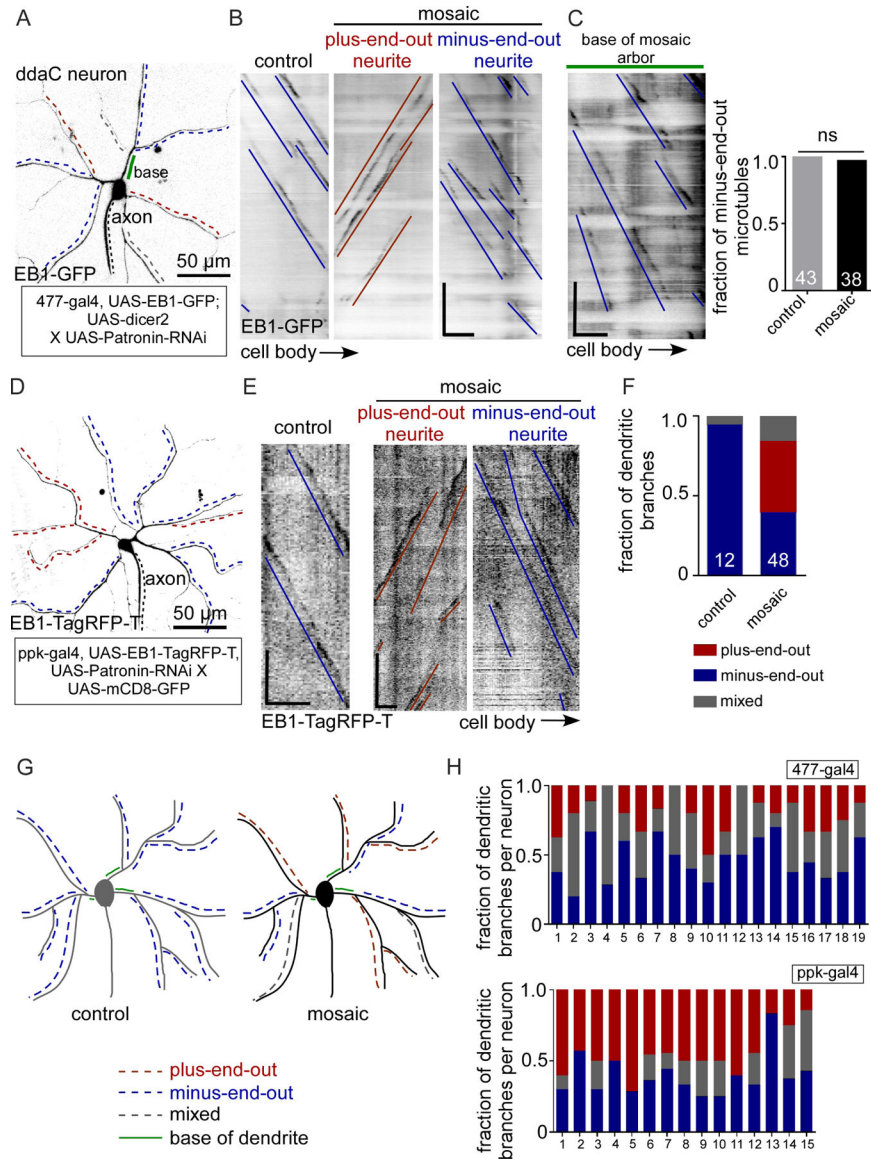
Figure 7. Plus-end-out neurites in mosaic arbors have reduced branching.

A. Representative images of control and mosaic ddaC neurons expressing the mCD8-GFP to visualize morphology. Secondary branches (quantified in B) are marked with purple dashed lines. Terminal branches (quantified in C) are marked with orange lines. In mosaic neurons microtubule polarity of neurites is marked with blue dashed lines for minus-end-out and red dashed lines for plus-end-out.

B. Quantification of the length of secondary branches in plus-end-out and minus-end-out neurites of mosaic neurons. ns, P>0.05 when analyzed with student's t-test (n=12 animals).

C. Quantification of the number of terminal branches (normalized to length) in plus-end-out and minus-end-out neurites in mosaic arbors. **, P<0.01 when analyzed with student's t-test (n=12 animals).

D. Representative kymographs from time-lapse videos of neurites in mosaic arbors expressing EB1-TagRFP-T. Blue lines mark the minus-end-out microtubules while red lines mark the plus-end-out microtubules. Scale bar: x axis = 10 μm, y axis = 60 seconds.

Resources table

Fly strain	Source or Reference	used in paper for
UAS-Patronin-RNAi (mosaic) on 3	#36659 from Bloomington Drosophila Stock Center (BDSC)	Fig. 1C, D
477-gal4, UAS-EB1-GFP/Cyo; UAS-dicer2/TM6	UAS-EB1GFP on 2 from Tadashi Uemura, 477-gal4 from Wesley Grueber, UAS-dicer2 from BDSC (#24650)	Fig. 1, Fig.4, Fig. 5
UAS-gamma-tubulin37c-RNAi (control)	#25271 from VDRC	Fig. 1C
ppk-gal4, UAS-EB1-TagRFP-T/TM6 (control)	Feng et al., 2019	Fig. 2, 3, 7
ppk-gal4, UAS-EB1-TagRFP-T, UAS-Patronin-RNAi/TM6 (mosaic)	tester line constructed for this study, UAS-EB1-TagRFP-T from Feng et al., 2019, ppk-gal4 from Wesley Gruebe	All figures except Fig.5
UAS-ANF-GFP	P{UAS-preproANF-EMD}136.3 7001 from David Deitcher, Wong et al., 2012	Fig.2
UAS-YFP-L10	Rolls et al., 2007	Fig.3
UAS-tdEos-alpha-tubulin on 2	Lu et al., 2013 (Gelfand lab)	Fig.4
UAS-mCD8-GFP on 2	#5137 from BDSC	Fig.6
UAS-iBlueberry on 3	#64187 from BDSC	Fig.4
Software	**Source or Reference**	
FIJI - ImageJ	National Institutes of Health: https://fiji.sc/	All figures
GraphPad Prism 7	https://www.graphpad.com/scientific-software/prism/	All figures